

Machine Learning Algorithms in Design Optimization

Daniele Peri

CNR-IAC – National Research Council
Istituto per le Applicazioni del Calcolo "Mauro Picone"
Via dei Taurini 19, 00185 Rome, Italy
d.peri@iac.cnr.it

September 7, 2022

Abstract

Numerical optimization of complex systems benefits from the technological development of computing platforms in the last twenty years. Unfortunately, this is still not enough, and a large computational time is necessary for the solution of optimization problems when mathematical models that implement rich (and therefore realistic) physical models are adopted.

In this paper, we show how the combination of optimization and Artificial Intelligence (AI), in particular Machine Learning algorithms, can help, strongly reducing the overall computational times, making also possible the use of complex simulation systems within the optimization cycle. Original approaches are proposed.

1 Introduction

The very first obstacle to the solution of an optimization problem is represented by the required time. In practice, the optimization task needs to be included inside the design activities schedule, and a specific time window is assigned. Consequently, the efficiency of the optimization algorithm is very important, and the number of attempts (computations of the objective

function) before the optimal configuration is identified has to be minimized. But, although the efficiency of the optimization algorithm is high, the time required for a single evaluation of the objective function could be so large that some compromises regarding the quality of the physical model become unavoidable: consequently, only a simplified mathematical model can be applied in practice, and the final solution is vitiated by this assumption.

For this reason, the use of interpolation/approximation algorithms has been widely adopted, particularly in the field of Multidisciplinary Design Optimization (MDO), where a cascade of several solvers, one for each discipline involved, are adopted together, greatly increasing the overall calculation time [1]. The first group of examples is given in [2, 3], more recently other applications can be found in [4, 5]. A review can be also found in [6]. In general, the base idea is the generation of a *meta-model*, that is, a *model of the model*, so that an estimate of the objective function can be obtained by using a simple closed-form expression. A *meta-model* can be represented by a polynomial model [7, 8] or something more flexible and sophisticated [9, 10, 11].

A great debate about the feasibility of a global interpolation/approximation model for a function of several variables is still on the table, particularly in the case of a large number of parameters. A sequence of local approximations has been soon proposed in [12], and other techniques in the same framework can be observed in [13, 14, 15, 8]: the objective is the reduction of the spatial validity of the interpolation, localizing the estimate. On the other side, the ambitious goal of building a single interpolation/approximation model for simulating the state of a system is the typical objective of Artificial Intelligence (AI), and those techniques, suitable for the management of a great amount of data, can be also adopted for the description of the digital twin of our physical system.

In this paper, we are describing some techniques able to provide a global interpolation of the state of a system as a function of the influencing parameters. A further improvement of the *meta-model* is then obtained by increasing the number of samples of the objective function in some critical areas, where the disagreement between the *meta-model* and the true value of the objective function is hypothesized to be high. A regularization technique is also introduced. The usefulness of these techniques is finally demonstrated thru the application to the solution of realistic design optimization problems.

2 Machine Learning for the *meta-model* improvement

As previously noticed, a central point for the optimization of complex systems can be represented by the determination of a simplified surrogate of a detailed mathematical model of the full system. We are referring to this as *meta-model* because it represents, in practice, *a model of the model*. Here we are recalling some topic elements of the building of the *meta-model*.

The first step for the definition of a *meta-model* is the generation of a dataset from which we can extract the information on the optimizing system. This is classically referred to as *Design Of Experiments* (DOE). Since we have typically no information about the function to be fitted, the DOE could be homogeneously distributed into the full Design Variable Space (DVS): for the generation of the DOE we can tap into the family of the so-called *Uniformly Distributed Sequences* (UDS). An equally-spaced DOE is also a guarantee of regularity of the resulting *meta-model*. Examples are the Halton/Hammersley sequences [16], Orthogonal Arrays [17], Latin Hypercube Sampling [18], Sobol sequence [19] and PT-Network [20].

Furthermore, one may be also interested in evaluating the credibility of the *meta-model* in off-design conditions, that is, the quality of the estimated output when a configuration different from the ones included in the DOE is checked. Classical theory of Artificial Neural Network (ANN) foresees the division of the DOE in two subsets, training set and validation set. The training set is used to produce the control parameters of the ANN, the validation set is used in order to measure the predictive qualities of the ANN.

Since we are considering numerical expensive models (in terms of computational time), the use of a set of data for validation purposes could appear as a waste of resources. It would be convenient to use all the available points for the determination of the parameters of the *meta-model*, without exceptions. By the way, if a UDS is adopted, the extraction of a single point is affecting the uniformity of the distribution.

Now we can add some new points for the determination of the performances of the system in some hypothetical configuration, not included in the training set: this way, we can obtain information about the degree of precision of the current version of the *meta-model*. Once used for their purposes, validation data should be then added to the training set, re-calibrating the *meta-model* with a richer quantity of information. This is what is commonly

called, in AI *Machine Learning* (ML), since we are using the original system (numerical or not) to learn something new to add to our AI system. This could become a very important phase of the formation of the *meta-model* if we could identify a specific area where it would be useful to add new points to the current *meta-model*. This is not easy, since the DOE is already uniformly distributed on the DVS, so the identification of a new sample cannot be performed based on purely geometric considerations (i.e., a specific region is not well covered by the training set).

A possible approach to this problem is proposed in [4]. If we compare different *meta-models* over the full DVS, we observe a different behavior among them, and we cannot determine *a priori* which *meta-model* is the best to apply. This situation is typical of a small DOE (undersampling). What we can do with a moderate computational cost is to compare systematically the outcome of different *meta-models* over the entire DVS, generating a denser UDS for this purpose, and then trace the disagreement between the prediction of the *meta-models*. We can interpret the discrepancy as a measure of the uncertainty in the prediction so that an additional training point where the disagreement is maximum will surely help in aligning locally the outputs of the *meta-models*. This is far different from adding a new point in an area with a low density of training points because this approach is explicitly considering the local quality of the approximation. Numerical experiments reported in [4] underline improvements of about 10% of the quality of the *meta-model* for the same number of training points: this is a demonstration that a uniform distribution of points in the training set is for sure a good start, but customization of the training set represents a more efficient solution.

3 Further tuning of the AI model

A regular distribution of the training points is a prerequisite for the determination of a response surface as regular. This means that loss of regularity in the distribution of training points can affect the regularity of the *meta-model* response surface, and the previously proposed algorithm is not preserving the regularity of the distribution: a regularization technique could be helpful in this context.

In the following, we are indicating a possible approach for *meta-models* whose construction implies the solution of a linear system. In particular, we

are considering Kriging [10, 4] and Multi-dimensional Spline [11].

3.1 Kriging regularization

The training of Kriging is performed by assembling and then factorizing the self-correlation matrix of the sample points [4]: the spatial correlation between two points of the DVS is determined uniquely based on the distance between the two points thru the so-called *semi-variogram* γ . In the original formulation, γ is computed experimentally, based on the available dataset. Once the experimental values of the *semi-variogram* are computed, a possible approach is to define γ as an exponential function obtained by fitting the experimental data, whose behavior is typically far from being regular. In theory, there is no reason why we should not define a different *semi-variogram* for each DOE point, so that we are indicating the local *semi-variogram* as

$$\gamma_i = e^{-(r/a_i)^2}$$

using different values of a_i , one for each point of the DOE. The coefficients a_i are the result of the fitting. γ_i are required for assembling the self-correlation matrix Γ , whose element $\Gamma_{i,j}$ represents the correlation between the i^{th} and the j^{th} sample point. If the coefficients a_i and a_j are different, Γ becomes unsymmetric. In practice, also due to the small amount of DOE points, a single *semi-variogram* is adopted and Γ is symmetric. Γ is then inverted, and the interpolation of the N DOE values $F(x_i)$ at the generic point x is obtained as

$$f(x) = \sum_{i=1}^N w_i F(x_i)$$

where the weights w_i are obtained by solving

$$\Gamma W = \Gamma_0$$

where Γ and Γ_0 are respectively

$$\Gamma = \begin{bmatrix} \gamma_1(0) & \gamma_1(r_{2-1}) & \dots & \gamma_1(r_{N-1}) & 1 \\ \gamma_2(r_{1-2}) & \gamma_2(0) & \dots & \gamma_2(r_{N-2}) & 1 \\ \dots & \dots & \dots & \dots & 1 \\ \gamma_N(r_{1-N}) & \gamma_N(r_{2-N}) & \dots & \gamma_N(0) & 1 \\ 1 & 1 & 1 & 1 & 0 \end{bmatrix} \quad \Gamma_0 = \begin{bmatrix} \gamma_1(r_{1-0}) \\ \gamma_2(r_{2-0}) \\ \dots \\ \gamma_N(r_{N-0}) \\ 1 \end{bmatrix}$$

and (r_{a-b}) is $\|\mathbf{x}_a - \mathbf{x}_b\|$. These formulas are used in the Best Linear Unbiased Prediction (BLUP) of random variables [21]. Under the assumption that the irregularities in the Kriging computation can be mainly addressed to the condition number of Γ , we can try to act on the coefficients of the *semi-variogram* a_i in order to maximize the condition number: a compass-search algorithm [22] is here applied, adjusting the coefficients a_i maximizing the condition number of Γ . A maximum variation of $\pm 50\%$ is allowed: at each step, a golden section search [23] is iteratively performed, so that the search limits are easily enforced.

In figure 1 we can see the effect of the regularization of Γ on the overall reconstruction of the objective function for a 2-dimensional closed form expression (Sasena function ¹). The use of a 2-dimensional function is here justified by the necessity of data visualization. In the first frame on left, we have the Kriging interpolation, where a single value of a_i , obtained by the standard fitting procedure, is applied; in the central frame, we can see the effect of the maximization of the condition number, with a different value of a_i for each sample point. In the extreme right frame, we have the effect of a minimization of the condition number. The effect of the maximization of the condition number is evident: the response surface is much more regular, in particular in the region between the sampled points or in the extreme regions, where there is not a sampled value. On the contrary, a minimization of the condition number is producing an interpolation formed by several Dirac-type regions, one for each sample point. It is evident how the criteria appear to be helpful in the regularization of the response surface.

3.2 Spline regularization

Also for Multi-Dimensional Spline (MDS), the weights are obtained through the solution of a linear system. Here the interpolation is obtained as a sum of N compact support functions $R(\rho)$, one for each sample point: also in this case can, the function can be different from each DOE point:

$$f(x) = \sum_{i=1}^N w_i R_i(\rho(x_i, x)) \quad (1)$$

where $\rho(x_i, x)$ is a measure of the distance between the i^{th} sample point

¹ $f(x) = 2 + 0.01 * (x_2 - x_1^2)^2 + (1 - x_1)^2 + 2 * (2 - x_2)^2 + 7 * \sin(0.5 * x_1) * \sin(0.7 * x_1 * x_2)$
 $x_1 \in [0, 5], x_2 \in [0, 5]$

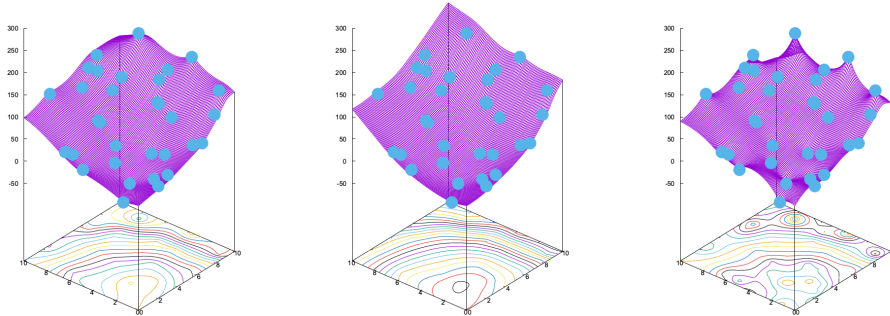


Figure 1: Effect of the tuning of Kriging on the base of the condition number of the self-correlation matrix Γ . On the left, the first guess, on the center the effect of a maximization of the condition number (that is, the proposed approach), and on right the effect of a minimization of the condition number (that is, the opposite of the proposed approach). The test has been performed using the Sasena function in \mathfrak{R}^2 . The function is sampled using 16 random points.

and the computational point x , and $R_i(\rho)$ is a compact support function, decreasing to zero at a certain distance from its center (the sample point). A simple expression for R , linear in the distance between the points, is

$$\begin{aligned}
 R &= 1 - b \|x_i - x\| \text{ for } b \|x_i - x\| \leq 1 \\
 R &= 0 \quad \text{otherwise}
 \end{aligned}$$

The weights of the kernel functions are determined by solving a linear system enforcing explicitly the equality between equation 1 and the sampled value at every point of the DOE. To compare with the previous case, while for Kriging the objective function was indirectly included through the *semi-variogram*, here it appears explicitly at the right end side of the linear system.

The parameter b represents a measure of the amplitude of the compact support function, and also this parameter can be adjusted for the improvement of the condition number of the matrix of the linear system to be solved,

using a procedure equivalent to the one previously described. The effect of the tuning is reported in figure 2. Compared with Kriging, MDS tends to produce a smoother response surface probably because the weights have a direct link with the local value of the objective function, and there is a progressive passage between the different influence areas of the DOE points when we move across the DVS. As observed in the left frame of figure 2, the case where all the b_i s are all equal was already regular. The differences between the first case and the regularized one are not so large as in the Kriging example, but they can still be observed looking at the contour levels reported at the bottom of the plot: a more regular behavior is evident in the neighborhood of the minimum of the function. As a further check, a comparison with the contour lines in figure 1 and figure 2 indicates that the effect of the regularization of MDS is also going in the direction of a stricter similitude with Kriging.

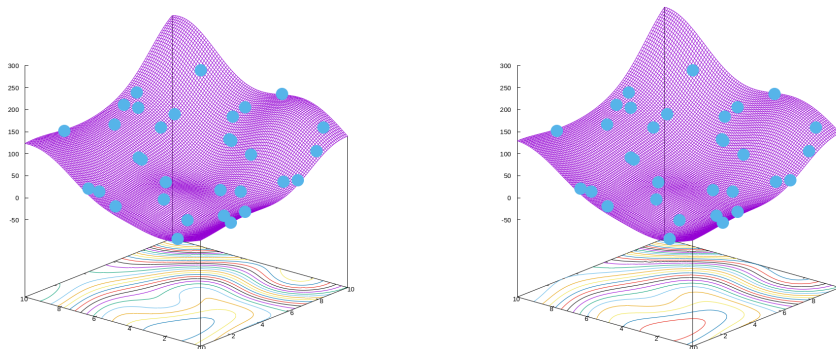


Figure 2: Effect of the tuning of MDS on the base of the condition number of the variance of the coefficients. On the left, is the first guess, and on right is the effect of tuning. The test has been performed using the Sasena function in \mathcal{R}^2 . The function is sampled using 16 random points.

4 Optimization algorithm

Meta-models (MM) and ML can be used as base elements for the definition of an optimization algorithm where the recourse to the mathematical model providing the value of the objective function is very limited. This is a situation absolutely valuable when the computational cost of a single value of the objective function is very high. Furthermore, since we are now dealing with a computationally inexpensive surrogate of the objective function, we can also avoid the recourse to a sophisticated optimization algorithm, proceeding by using a *brute force* approach, where the DVS is sampled extensively by using the MM. The algorithm can be depicted sketchily by the pseudocode reported in **Algorithm 1**.

Algorithm 1 PSI-AI algorithm

```
Perform initial sampling (DOE)
for  $N_E < N_E^{max}$  do
  Apply ML
  Search the DVS using MM
  Update DOE
  Center the DVS on the current best solution
  Reduce the amplitude of DVS
end for
```

N_E is the current number of objective function evaluations, and N_E^{max} is the maximum effort we want to put into the search, measured as the maximum number of evaluations of the objective function we are willing to perform. The name PSI-AI comes from the original formulation of the so-called Parameter Space Investigation (PSI) originally proposed in [20] but without the ML improvement phase.

The initial sampling of the DVS is performed by using a uniform distribution of points: this is in the logic of the uniform probability that every point of the DVS could host the optimal value of the objective function unless some information on the objective function is gained. The DOE is obtained using a $P\tau$ -net distribution, extensively reported in [20].

A relevant parameter is represented by the constriction factor (< 1), that is, the amount of reduction of the DVS amplitude when we are passing from one iteration to another. A small value means a strong reduction: in this case, the convergence toward the more promising area is fast, but we can lose

the location of the global minimum due to premature focalization. On the contrary, a large value, close to 1, is a guarantee of the completeness of the exploration, but it can require a very large number of iterations (and then a large number of evaluations of the objective function) to get the convergence. Here we are performing a comparative study about the role of this parameter. In figure 3 the effects of a systematic variation of the constriction parameter α are reported. A quadratic function of 12 variables is here minimized²: the DOE is composed of 192 points ($16\times$ the number of design variables), and at each iteration, 8 further points are added during the ML phase, while the best 8 points selected on the base of the evaluation of a regular sampling of the DVS using the MM are also added at each iteration. 10 iterations are performed. In the picture, to focus on the convergence of the algorithm, the representation of DOE evaluation is not included. We can observe from figure 3 that a value of $\alpha = 0.5$ causes a premature convergence, and the reduction of the objective function is quite large but also far from the best value. A value of α in between 0.8 and 0.9 appears to be the most appropriate choice, with a slight preference for 0.9, since it looks like a further improvement of the objective function would be possible if a larger number of iterations were allowed. Larger values appear to slow down too much the convergence of the algorithm, although they are a guarantee (asymptotically) of a more accurate exploration of the DVS.

² $f(x) = \sum_{i=1}^{12} (x_i - 0.5)^2 \quad x_i \in [-10 : 10]$

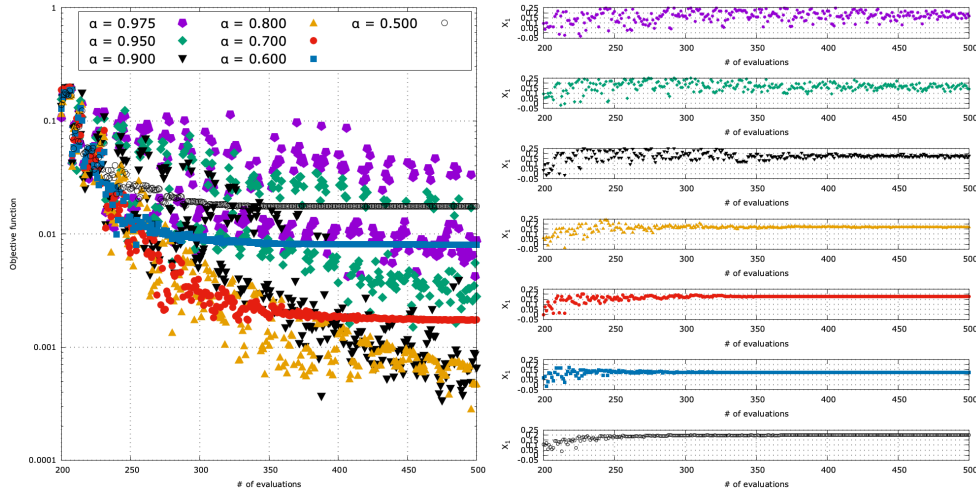


Figure 3: Effects of different values of the constriction factor on the convergence of the PSI-AI algorithm. On the left panel, the percentage difference between the current best value of the objective function and the optimal value, and on the right panel the numerical value of the first (of 12) design parameter: different graphs are for different values of the constriction factor, with colors in accordance with the left side picture. On the horizontal axis, in every graph, the current number of objective function evaluations.

5 Application to realistic problems

To check the qualities of the algorithm on a realistic application, whose resulting objective function is possibly not showing a single clear global minimum as in the adopted algebraic test case, the problem of the optimization of a monohull ship has been considered. The parent hull form (PHF) for the ship design optimization has been taken from [24]: it represents the bare hull geometry of a *Vaporetto*, the water-bus performing public transport in Venice. Lines and main dimensions are reported in figure 4.

5.1 Pitch motion reduction

As a first case study, the PSI-AI algorithm has been compared with an efficient multi-agent optimization algorithm, to understand and evaluate the performance we can expect from PSI-AI. The selected optimization algo-

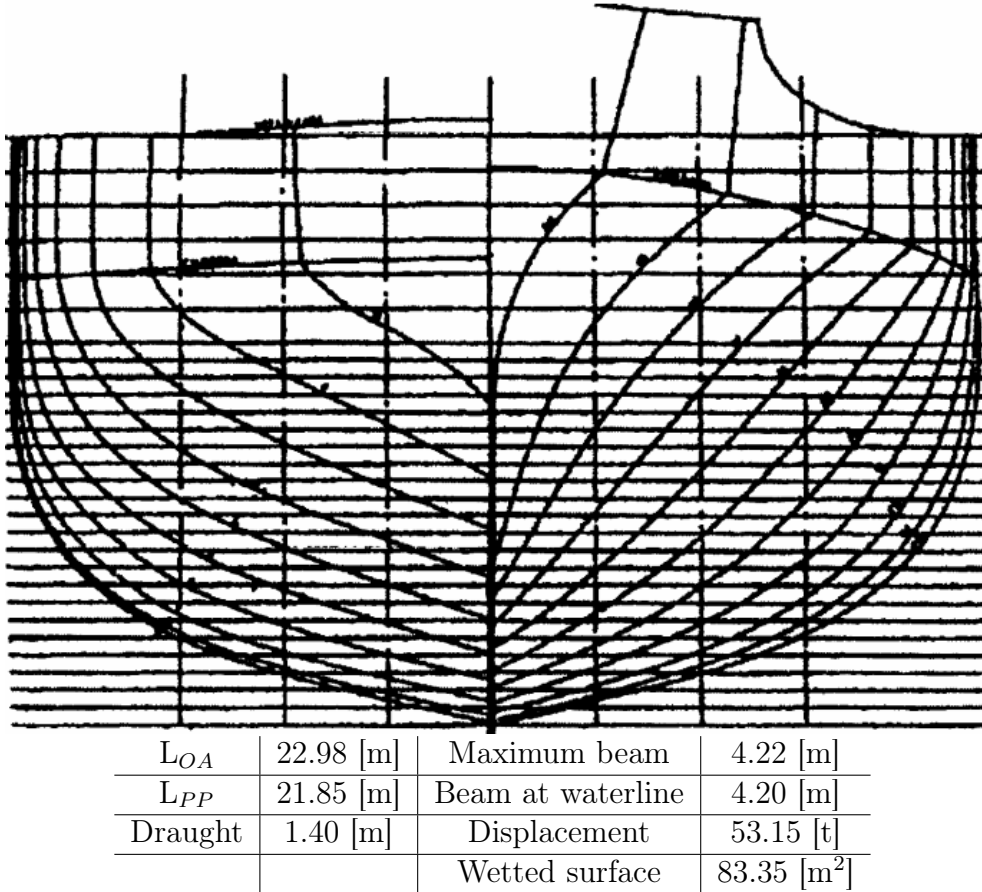


Figure 4: Section lines of the *Vaproetto* as from [24].

rithm is the hybrid version of the Imperialist Competitive Algorithm (ICA), originally proposed in [25] and then here adopted in the improved version [26] as **hICA**. The **hICA** includes also a local search algorithm, used in conjunction and in cooperation with the original multi-agent algorithm. **hICA** has been proved to be more efficient than other multi-agent algorithms, like the NSGA-II implementation [27] of a Genetic Algorithm (GA)[26].

To limit the computational effort, the energy associated with the pitch response of the ship in rough seas has been considered as objective function. This choice allows the application of a very fast (but reliable) simulation tool, the open-source **PDStrip** seakeeping code [28]. The objective function

is represented by the area below the RAO pitch curve, at the speed of 10 knots. Its evaluation has a computational cost lower than 9 seconds on a 3.30GHz Intel®Core™i7-5775R: as a consequence, we can easily perform extensive tests in a reasonable time.

The parameterization of the hull has been produced by using the Free Form Deformation (FFD) approach, proposed and described in [29]. A patch with $5 \times 4 \times 6$ subdivisions (respectively along the \mathbf{X} , \mathbf{Y} and \mathbf{Z} Cartesian axes) has been adopted, but only 12 control points are active: the first and the last planes along the \mathbf{X} direction are kept fixed, as well as three first slices in the \mathbf{Y} direction together the bottom plane and the first two top planes in the \mathbf{Z} direction. Only the 4×3 control points on the last lateral slice parallel to the \mathbf{XZ} plane can freely move along the lateral direction, their movement is limited to 25 centimeters (ship scale). The patch is including the PHF geometry up to the plane $z = 1.5$ meters, in order not to change the bridge geometry: the fixed control points of the FFD enforce the continuity between the modified and unmodified parts of the hull. An example of possible deformation obtained with this configuration is reported in figure 5.

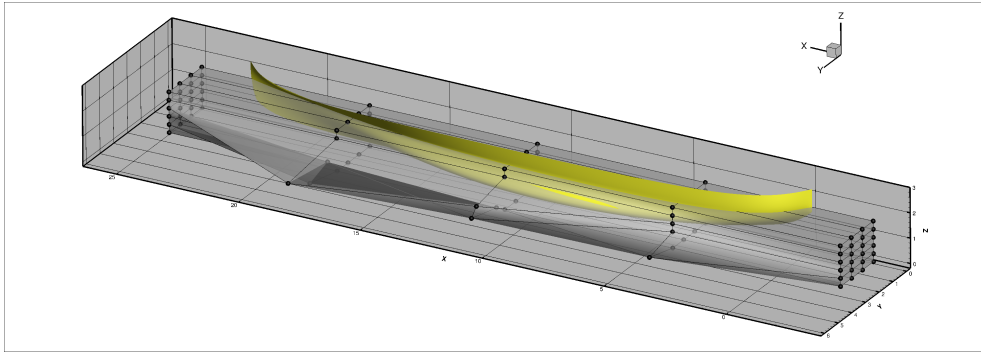


Figure 5: Example of shape deformation of the *Vaporetto* geometry. The hull is partly embedded into a single FFD patch, leaving unchanged the top part of the ship. Here the deformation producing the optimal shape is reported. Black dots are the control points of the FFD, while the hull shape is represented in yellow. Bow points toward the positive direction so that we are here observing the hull from the stern.

Among the different possible choices, Kriging has been adopted as a substitute for the mathematical model, while the MDS has been adopted for the

ML phase together with Kriging.

The results, in terms of the objective function and design parameters, are reported in figure 6. Here is clear how the number of objective function evaluations required to reach convergence for **PSI-AI** is about one-third with respect to **hICA**. On the other hand, we have some differences in the optimal values of the design parameters, whose numerical values are reported in table 1.

Firstly we analyze the evolution of the design parameter values thru the optimization procedure. We can clearly observe how the optimal values of the design parameters in many cases are similar, but not in all the cases. Since most of the parameters find their optimum value on the border of the admissible portion of the DVS, we can argue that there is not a stationary point in the constrained DVS, so the selected optimum is the one producing the best possible value of the objective function, but the local derivatives of the objective function are not null. This situation is clear for 9 out of 12 parameters. For the remaining 3 parameters (#4, 8, and 12), the difference is mainly addressable to their small sensitivity of the objective function: in fact, the final value of the objective function for the two optimal points is absolutely comparable. The two algorithms have different attitudes in the exploration of the DVS. In **PSI-AI** the search has not a preferential area, and the focusing is progressive, and the initial search is mainly grounded on the center of the DVS. On the contrary, the **hICA** generally expands towards the extreme regions of the admissible DVS, eventually resizing the group of the agents in a second moment. As a consequence, if the sensitivity of a parameter is small, **PSI-AI** will preferentially return a value not close to the borders of the admissible DVS, while **hICA** is implicitly encouraging the values at the extremes.

Table 1: Optimal values of parameters obtained using the two different optimization algorithms, **PSI-AI** and **hICA**. The two sets of parameters are represented side-by-side, ordered by the number of the design parameter.

#	hICA	PSI-AI	#	hICA	PSI-AI	#	hICA	PSI-AI
1	0.2490	0.2432	2	0.2484	0.2498	3	0.2495	0.2499
4	-0.2454	0.2045	5	0.2441	0.2498	6	0.2499	0.2500
7	0.2486	0.2496	8	-0.2494	0.1592	9	0.2490	0.2484
10	0.2455	0.2485	11	0.2493	0.2412	12	0.1957	0.2105

This hypothesis is substantially confirmed by the results of the sensitivity

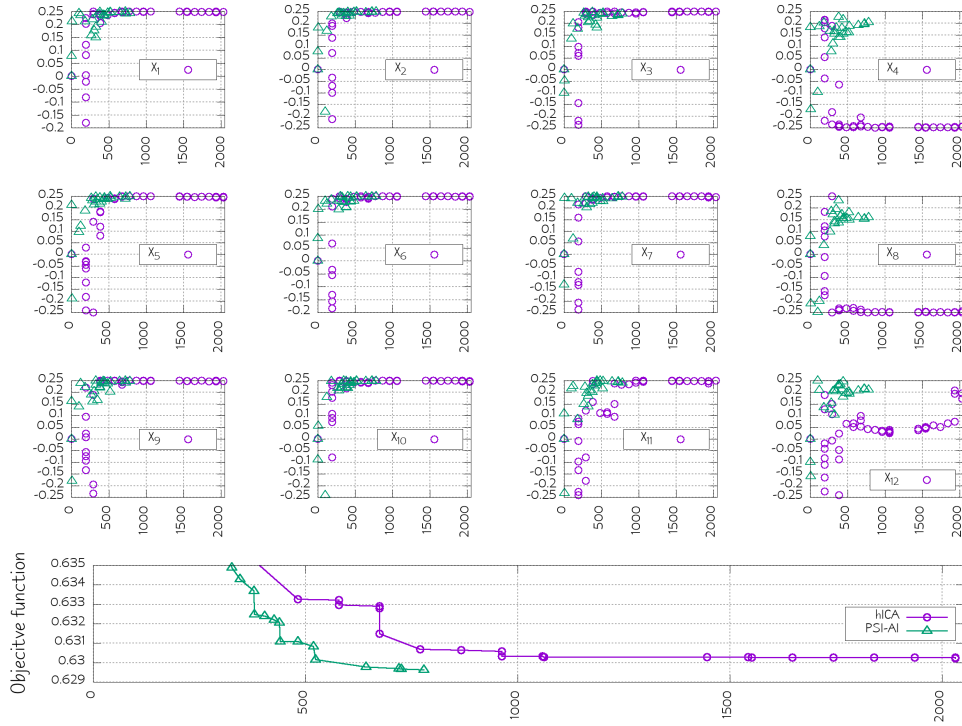


Figure 6: Comparison between the PSI-AI approach and the hICA algorithm. On the top, is the time history of the 12 design variables. On the bottom, the progressive reduction of the objective function value thru the iterations. A dot is plotted only if an improvement of the objective function occurs.

analysis reported in figure 7. In this picture, a single parameter is changed at a time, revealing the influence of each parameter on the objective function. Here we can observe how there is a small group of design variables with a reduced sensitivity with respect to the objective function: all the previously listed parameters belong to this group. As a consequence, the small influence of these parameters is the reason why they are much more prone to follow the tendency subtly suggested by the algorithm.

In figure 8 the progressive reduction of the discrepancies between the two adopted MMs during the course of the optimization process is reported. The full number of calls to the objective function is about 800: this means that only a quarter of them are devoted to the ML algorithm. After 80

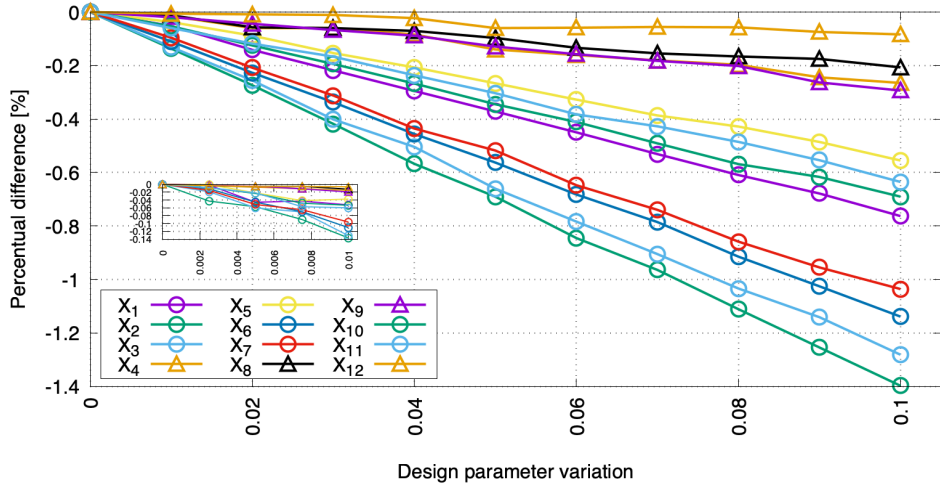


Figure 7: Sensitivity analysis of the pitch peak as a function of the design parameters. In the sub-picture, the detail of the effect of smaller variations of the design parameters: here the horizontal scale is about one-tenth of the larger picture.

evaluations, the difference is of the order of 1%: this can be considered a relevant achievement, demonstrating the efficiency of the ML algorithm.

5.2 Total resistance

A second test case has been produced to further check the capabilities of the PSI-AI algorithm. The objective function is now represented by the effective power in calm water of the *Vaporetto* at the speed of 4.5 m/s, which is a little lower than the maximum speed fixed by the rules (20 km/h). Due to the motivations of the present work, the shape of the sea bottom and the side walls of the channels have been not considered, although they are peculiar elements for this kind of sea vehicle traveling in the Venice area. Hydrodynamic computations are performed using a single-layer potential flow solver, of the class of the Boundary Element Methods (BEM) [30]. These kinds of solvers are correctly modeling the wave pattern generated by the hull, but the viscous effects are not included in the formulation, so they are introduced *a posteriori* in a simplified way. The resulting estimate of the effective power has been proved to be reliable, at least from the engineering point of view.

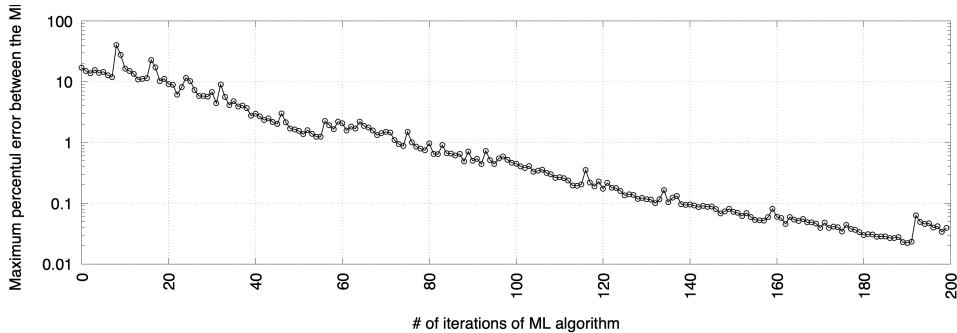


Figure 8: Effect of the Machine Learning algorithm on the relative precision of the two different *meta-models*. On the horizontal axis, the number of calls to the objective function required by the ML algorithm during the optimization problem, on the vertical axis the maximum value across the full DVS of the percentage difference in the prediction of the two different *meta-models*. A reduction of the discrepancies is a guarantee of the reliability of the interpolations.

The computational effort of a fully-3D BEM is larger than a strip-theory method, also because computations need to be repeated iteratively to obtain the actual values of the sinkage and trim of the ship. The CPU time for a single value of the objective function is now about 40 seconds on the same computational platform. For this reason, the comparison with the `hICA` algorithm has been not repeated.

The same parameterization as from the previous test case has been adopted, including also the constraints on the design variables.

At the end of the optimization problem, the effective power required by the *Vaporetto* is passing from 22.44 to 15.10 kW, with a reduction of 32.72%. To have a second check of the improvements, the RANSE solver `interFoam`, from the suite `OpenFOAM`[31] has been also applied: results are reported in table 2, where we can see the substantial equivalence of the estimated percentual reductions (34.1 vs. 32.7%). In this case, the Reynolds-averaged Navier-Stokes equations, including explicitly the viscous terms neglected in the Laplace equation of the BEM method, have been solved. Also `interFoam` is taking into account the real sinkage and trim of the hull.

Figure 9 is reporting the changes in the shape of the PHF. The beam is increased, and a part of the volume is shifted fore: since the displacement is

Table 2: Optimal values of the wave resistance, frictional resistance, and total resistance for the original and optimized hulls, computed by using the RANSE solver `interFoam` from the suite `OpenFOAM`©[31]. The simulations are performed with the hull able to take the dynamic sinkage and trim. Since the effective power differs by the total resistance by a constant, the percentage differences of total resistance are the same as the ones of the effective power.

Ship	R_W [N]	R_F [N]	R_T [N]
Original	2411.0	430.9	2841.9
Optimal	1638.9	234.7	1873.6
$\Delta\%$	-32.0	-45.5	-34.1

fixed, the draught of the optimal hull is smaller in comparison with the PHF one. The topside of the hull is not changing: as a consequence, the beam increase is causing a kind of lateral bulb in the central part of the ship. If required, the hull lines of the out-of-the-water part of the hull, not directly influencing the performance, can be reassessed to have a more regular shape. The red color on the hull geometry is evidencing the wetted part of the hull at the optimizing speed.

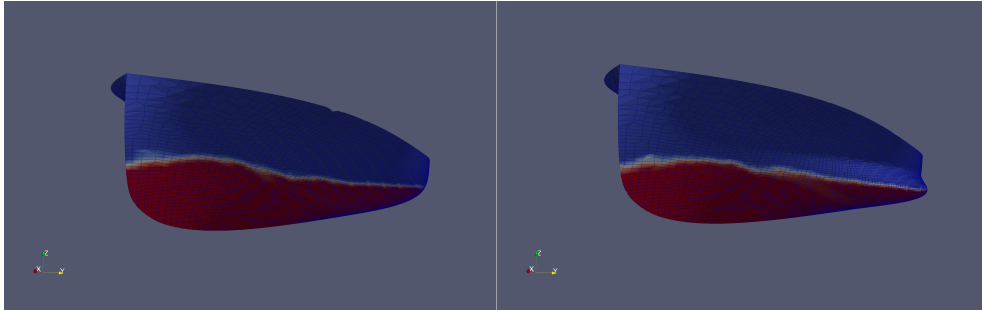


Figure 9: Perspective view of the PHF (on left) and the optimal (on right) hull shapes. The red color is indicating the wetted part of the hull (as computed by using the `interFoam` RANSE solver).

In figure 10 we have reported a different way to stress the increasing similitude between the prediction of the two MMs as the ML iterations are going on. The two MMs have been computed on a large number of points laying into the DVS: on each frame, we have on the horizontal axis the

estimate provided by Kriging, while the estimate by MDS is reported on the vertical axis. If the values estimated by two MMs were the same, all the points would be aligned along the $x = y$ line in the plot. If the points are not well aligned, there is still a difference between the prediction of the two MMs. We can see how, proceeding from left to right, top to bottom, the points are thickening on the line of full correlation: this is a sign of a progressive increase in the coherence between the two MMs. Since all the points are aligned, the similitude of the two MMs is certified on the full DVS.

In figure 11 and 12 we have a snapshot of the wave pattern produced by the PHF and the optimal hull. Figure 11 reports the differences between the wave profile on the hull (and on the centerplane) as simulated by the BEM solver. In the picture, the hull is located in between $x = -0.5$ and $x = 0.5$, with the bow at $x = -0.5$. The optimal hull shows a more regular wave pattern along the hull, and the hollow observed in the rear part of the PHF has disappeared. In the wake, the wave profile is reduced after optimization, which is typically beneficial.

The same conditions have been also simulated by using a RANSE mathematical model, with richer physical content. Results are substantially confirmed, as previously mentioned. Here we can compare the wave pattern predictions: in figure 12 we can see a top view of the wave pattern and a comparison of a longitudinal wave cut, for both the PHF and optimal configuration. The position of the longitudinal cut is reported as a black line in the upper frame of the same picture. The reduction in the wave elevation along the hull and in the region close to the stern is clearly evident. We cannot completely exclude that part of the great success of the optimization activities could be possibly connected with a slightly inaccurate reproduction of the linesplans of the real PHF shape (both in the drawings reported in [24] and/or in the digitalized ones), so that the performances of the PHF are lower than reality.

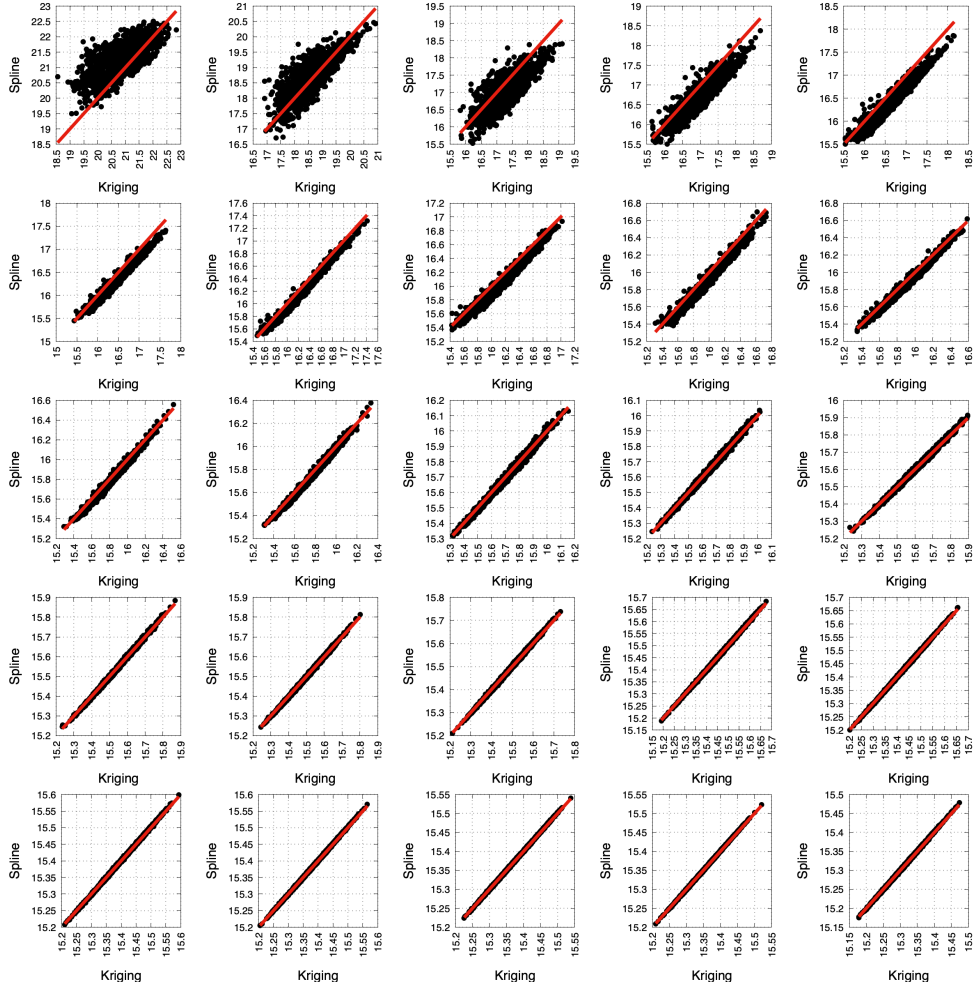


Figure 10: Effect of the application of the ML algorithm on the overall precision of the adopted *meta-models*. In each framework, the values of the objective function as predicted by the two different *meta-models* at a specific iteration are reported on the two axes. Iteration number (frame number) is running from left to right, top to bottom.

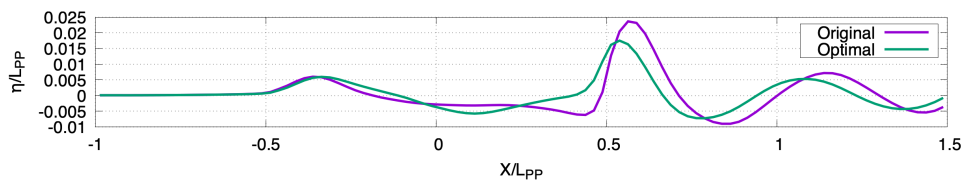


Figure 11: Comparison between wave pattern generated by the PHF and optimal hulls, computed with the BEM solver [30], the one applied for the evaluation of the objective function. The ship hull is placed in between $x = -0.5$ and $x = 0.5$, with bow at $x = -0.5$.

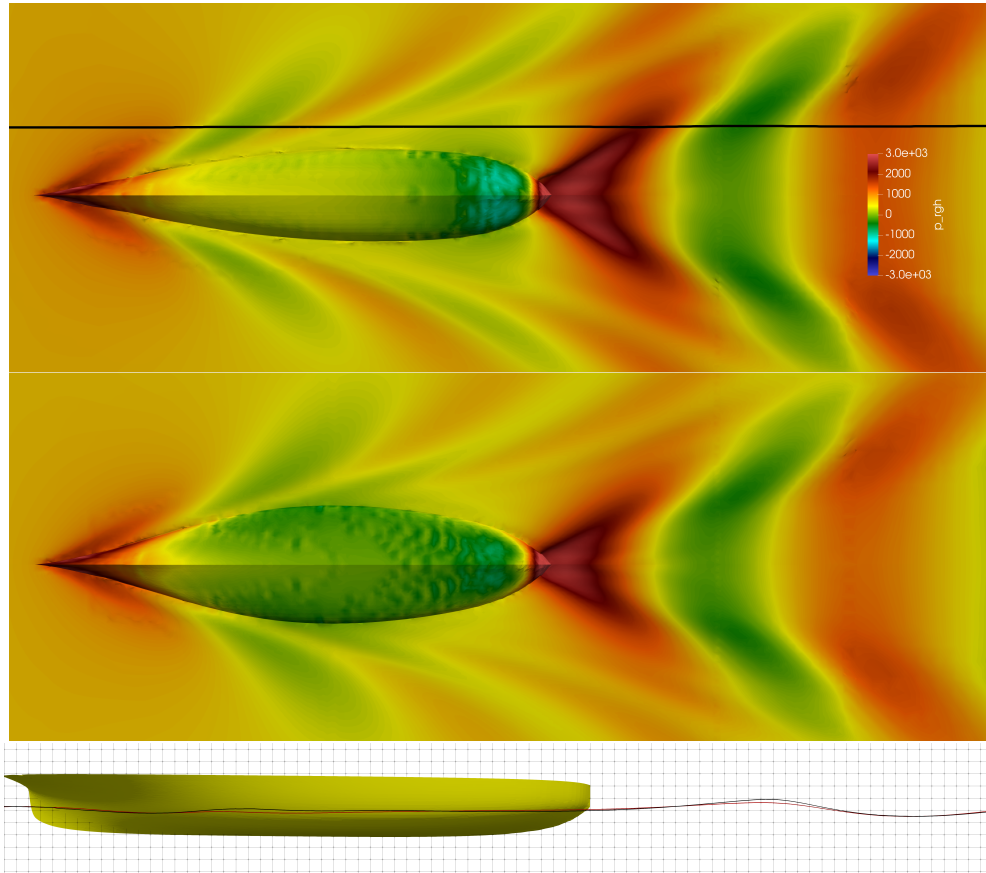


Figure 12: Comparison between wave pattern generated by the PHF and optimal hulls, computed by using the RANSE solver `interFoam` from the suite `OpenFOAM`©[31]. On top, is the top view of the wave patterns, where the optimal hull is presented in the lower part. On the bottom, is the comparison of a longitudinal wave cut of the PHF (black) and optimal (red) hulls. The trace of the cut is reported as a black line in the top view.

6 Conclusions

The paper is evidencing the connections between AI and optimization, demonstrating how some techniques classically adopted in AI can be easily and fruitfully applied as base elements of an optimization algorithm. There are some limitations, mainly connected with the space dimensionality of the problem: in fact, to consider a large number of design parameters may imply the requirement of a very large DOE, causing at the same time a huge computational cost for the training of the MM. This situation may become even harder if the objective function is multimodal so that the number of points required for the synchronization of the prediction of the MMs during the ML phase becomes also larger than in the present cases. In these conditions, the use of the classical optimization approach could still represent a more viable solution.

More experiences are needed to better establish the limits of the approach. Also, the use of more than a couple of MM, to further improve the tuning phase, could be investigated.

Acknowledgements

This research was funded by Italian Minister of Instruction, University and Research (MIUR) to support this research with funds coming from PRIN Project 2017 (No. 2017KKJP4X entitled "Innovative numerical methods for evolutionary partial differential equations and applications").

Conflict of interest

The authors declare that they have no conflict of interest.

References

- [1] R. T. Haftka, J. Sobieszczanski-Sobieski, S. L. Padula, On options for interdisciplinary analysis and design optimization, *Structural Optimization* 4 (2) (1992) 65–74.
- [2] V. Toropov, Multipoint approximation method in optimization problems with expensive function values, in: *Proceedings of the 4th International*

Symposium on Systems Analysis and Simulation, Elsevier Science Inc., USA, 1992, p. 207–212.

- [3] J.-F. Barthelemy, R. T. Haftka, Approximation concepts for optimum structural design - a review, *Structural Optimization* 5 (3) (1993) 129–144.
URL www.scopus.com
- [4] D. Peri, Self-learning metamodels for optimization, *Ship Technology Research* 56 (3) (2009) 95–109.
- [5] F. Viana, T. W. Simpson, V. Balabanov, V. Toropov, Metamodeling in multidisciplinary design optimization: How far have we really come?, *AIAA Journal* 52 (4) (2014) 670–690.
- [6] A. Parnianifard, A. Azfanizam, M. K. A. M. Ariffin, M. I. S. Ismail, N. A. Ebrahim, Recent developments in metamodel based robust black-box simulation optimization: An overview, *Decision Science Letters* 8 (1) (2019) 17–44.
- [7] R. H. Myers, D. C. Montgomery, C. M. Anderson-Cook, *Response surface methodology: process and product optimization using designed experiments*, John Wiley & Sons, 2016.
- [8] D. Peri, F. Tinti, A multistart gradient-based algorithm with surrogate model for global optimization, *Communications in Applied and Industrial Mathematics* 3 (2012) 1–22.
- [9] T. Poggio, F. Girosi, Networks for approximation and learning, *Proceedings of the IEEE* 78 (9) (1990) 1481–1497. doi:10.1109/5.58326.
- [10] G. Matheron, Principles of geostatics, *Economic Geology* 58 (8) (1963) 1246–1266.
- [11] D. Peri, Easy-to-implement multidimensional spline interpolation with application to ship design optimisation, *Ship Technology Research* 65 (1) (2018) 32–46. arXiv:<https://doi.org/10.1080/09377255.2017.1407545>, doi:10.1080/09377255.2017.1407545.
URL <https://doi.org/10.1080/09377255.2017.1407545>

- [12] N. M. Alexandrov, J. E. Dennis, R. M. Lewis, V. Torczon, A trust-region framework for managing the use of approximation models in optimization, *Structural and Multidisciplinary Optimization* 84 (14) (1992) 65–74.
- [13] J. R. C. Wei, S. T. W, Comparative studies of metamodeling techniques under multiple modeling criteria, *Structural and Multidisciplinary Optimization* 23 (1) (2001) 1–13.
- [14] E. Acar, M. Rais-Rohani, Ensemble of metamodels with optimized weight factors, *Structural and Multidisciplinary Optimization* 37 (3) (2009) 279–294. doi:10.1007/s00158-008-0230-y.
URL <https://doi.org/10.1007/s00158-008-0230-y>
- [15] R. Teixeira, M. Nogal, A. O’Connor, Adaptive approaches in metamodel-based reliability analysis: A review, *Structural Safety* 89 (2021) 102019. doi:<https://doi.org/10.1016/j.strusafe.2020.102019>.
URL <https://www.sciencedirect.com/science/article/pii/S0167473020300989>
- [16] J. H. Halton, G. B. Smith, Algorithm 247: Radical-inverse quasi-random point sequence, *Communications of the ACM* 7 (12) (1964) 701–702. doi:10.1145/355588.365104.
URL <https://doi.org/10.1145/355588.365104>
- [17] A. S. Hedayat, N. J. A. Sloane, J. Stufken, *Orthogonal Arrays: Theory and Applications*, Springer-Science+Business Media, 1999. doi:10.1007/978-1-4615-2089-4.
- [18] M. D. McKay, Latin hypercube sampling as a tool in uncertainty analysis of computer models, in: R. C. Crain (Ed.), *Proceedings of the 24th Winter Simulation Conference*, Arlington, VA, USA, December 13-16, 1992, ACM Press, 1992, pp. 557–564. doi:10.1145/167293.167637.
URL <https://doi.org/10.1145/167293.167637>
- [19] P. Bratley, B. L. Fox, Algorithm 659: Implementing sobol’s quasirandom sequence generator, *ACM Trans. Math. Softw.* 14 (1) (1988) 88–100. doi:10.1145/42288.214372.
URL <https://doi.org/10.1145/42288.214372>

- [20] R. Statnikov, J. B. Matusov, *Multicriteria Optimization and Engineering*, Springer-Science+Business Media, Dordrecht, The Netherlands, 1995. doi:10.1007/978-1-4615-2089-4.
- [21] G. K. Robinson, That BLUP is a Good Thing: The Estimation of Random Effects, *Statistical Science* 6 (1) (1991) 15 – 32. doi:10.1214/ss/1177011926.
URL <https://doi.org/10.1214/ss/1177011926>
- [22] E. Beale, On an iterative method for finding a local minimum of a function of more than one variable, *Statistical Techniques Research Group Technical Report 25*, Princeton University (1958).
- [23] J. C. Kiefer, Sequential minimax search for a maximum, *Proceedings of the American Mathematical Society* 4 (3) (1953) 502–506. doi:doi:10.2307/2932161.
- [24] I. Zotti, Applicazione delle serie sistematiche e verifica dei risultati, in: *Definizioni di metodi e strumenti necessari alla verifica dell’attitudine alla navigazione nella laguna di Venezia*, Università degli studi di Trieste, ITA, 2002, p. 1–65.
- [25] E. Atashpaz-Gargari, C. Lucas, Imperialist competitive algorithm: An algorithm for optimization inspired by imperialistic competition., in: *IEEE Congress on Evolutionary Computation*, IEEE, 2007, pp. 4661–4667.
- [26] D. Peri, Hybridization of the imperialist competitive algorithm and local search with application to ship design optimization, *Computers & Industrial Engineering* 137 (2019) 106069. doi:<https://doi.org/10.1016/j.cie.2019.106069>.
URL <https://www.sciencedirect.com/science/article/pii/S0360835219305285>
- [27] K. Deb, A. Pratap, S. Agarwal, T. Meyarivan, A fast and elitist multiobjective genetic algorithm: Nsga-ii, *IEEE Transactions on Evolutionary Computation* 6 (2) (2002) 182–197. doi:10.1109/4235.996017.
- [28] V. Bertram, B. Veelo, H. Söding, K. Graf, Development of a freely available strip method for seakeeping, in: *COMPIT*, Vol. 6, 2006, pp. 356–368.

- [29] T. W. Sederberg, S. R. Parry, Free-form deformation of solid geometric models, in: Proceedings of SIGGRAPH 86 conference, Dallas, USA, 1986, pp. 151–160.
- [30] G. E. Gadd, A method of computing the flow and surface wave pattern around full forms, Royal Institution of Naval Architects, Supplementar papers 118 (1976) 207–219.
- [31] T. O. Foundation, ©2011-2021 the openfoam foundation, <https://openfoam.org>, accessed: 2021-08-01 (2011).